Ming-Jay Chow
e-mail: jchow@bu.edu

Yu Zou
e-mail: zou@bu.edu

Department of Mechanical Engineering,
Boston University,
Boston, MA 02215

Huamei He
e-mail: hehhu@musc.edu

Francis X. McGowan, Jr.
e-mail: mcgowanf@musc.edu

Deparment of Anesthesia and
Perioperative Medicine,
MUSC Storm Eye Institute,
Charleston, SC 29403

David Zurakowski
Department of Anesthesiology,
Perioperative and Pain Medicine,
Children's Hospital Boston,
Harvard Medical School,
Boston, MA 02115
e-mail: david.zurakowski@childrens.harvard.edu

Yanhang Zhang[1]
Departments of Mechanical Engineering and
Biomedical Engineering,
Boston University,
110 Cummington Street,
Boston, MA 02215
e-mail: yanhang@bu.edu

Obstruction-Induced Pulmonary Vascular Remodeling

Pulmonary obstruction occurs in many common forms of congenital heart disease. In this study, pulmonary artery (PA) banding is used as a model for pulmonary stenosis. Significant remodeling of the vascular bed occurs as a result of a prolonged narrowing of the PAs, and here we quantify the biophysical and molecular changes proximal and distal to the obstruction. Main and branch PAs are harvested from banded and sham rabbits and their mechanical properties are assessed using a biaxial tensile tester. Measurements defined as initial and stiff slopes are taken, assuming a linear region at the start and end of the J-shaped stress-strain curves, along with a transitional knee point. Collagen, elastin assays, Movat's pentachrome staining, and Doppler protocols are used to quantify biochemical, structural, and physiological differences. The banded main PAs have significantly greater initial slopes while banded branch PAs have lower initial slopes; however, this change in mechanical behavior cannot be explained by the assay results as the elastin content in both main and branch PAs is not significantly different. The stiff slopes of the banded main PAs are higher, which is attributed to the significantly greater amounts of insoluble collagen. Shifting of the knee points reveals a decreased toe region in the main PAs but an opposite trend in the branch PAs. The histology results show a loss of integrity of the media, increase in ground substance, and dispersion of collagen in the banded tissue samples. This indicates other structural changes could have led to the mechanical differences in banded and normal tissue. [DOI: 10.1115/1.4005301]

Introduction

Pulmonary stenosis makes up approximately 10% of congenital heart defects and plays a role in many other congenital heart defects as well [1,2]. Characterized by a thickened pulmonary valve or narrowing of the pulmonary arteries, pulmonary stenosis results in increased myocardial work, dilation of coronary arteries, narrowed pulmonary arteries, and decreased blood flow to the lungs [3,4]. To study this important component of congenital heart defects, previous studies have used PA banding as a model for pulmonary stenosis. PA banding involves forming an obstruction of pulmonary blood flow by placing a temporary restricting band around the PA. The pressure gradient from the obstruction causes many of the same symptoms that are due to pulmonary stenosis [5–7].

While using PA banding as a model for pulmonary stenosis is well established, there are lack of studies that investigate the remodeling in the artery as a result of the formation of a pressure gradient. Several previous studies have investigated the changes in the right ventricle (RV), such as free wall thickness and cardiac fibrosis [8,9], while others have studied how specific isozymes contribute to cardiac remodeling [10]. In clinical situations, pulmonary stenosis can create a pressure gradient in the artery of around 20–60 mm Hg, and blood flow becomes turbulent distal to a stenosis [11,12]. It is commonly accepted that arteries remodel as a result of injury, disease, and changes in pressure/blood flow conditions. In the pulmonary circulation, hypertension has been shown to increase wall thickness and change artery composition and stiffness [13]. In systemic arteries, hypertension, aging, and diabetes can lead to structural remodeling in the form of increases in media thickness, extracellular matrix (ECM) components, collagen/elastin ratio, and changes in the structure of the elastic lamina [14–17]. Differences in the relative area of intima/media/adventitia, increased deposition of ECM and smooth muscle cells (SMCs), and disruption of the internal elastic lamina occur in carotid and coronary arteries as a result of changes in blood flow [18,19]. Due to the change in pressure and blood flow in the artery after introducing a pulmonary obstruction via PA banding, it is expected that there should be structural and mechanical changes in the artery.

The goal of this study is to understand the role of microstructural components in vascular remodeling by quantifying the changes in ECM structure after an obstruction and correlating these changes with the mechanical function of PAs. This information is important to unraveling the underlying key mechanisms of vascular remodeling and developing advanced mechanobiological constitutive models that integrate quantitative information of

[1]Corresponding author.

Contributed by the Bioengineering Division of ASME for publication in the JOURNAL OF BIOMECHANICAL ENGINEERING. Manuscript received June 13, 2011; final manuscript received September 29, 2011; published online December 8, 2011. Assoc. Editor: Jeffrey W. Holmes.

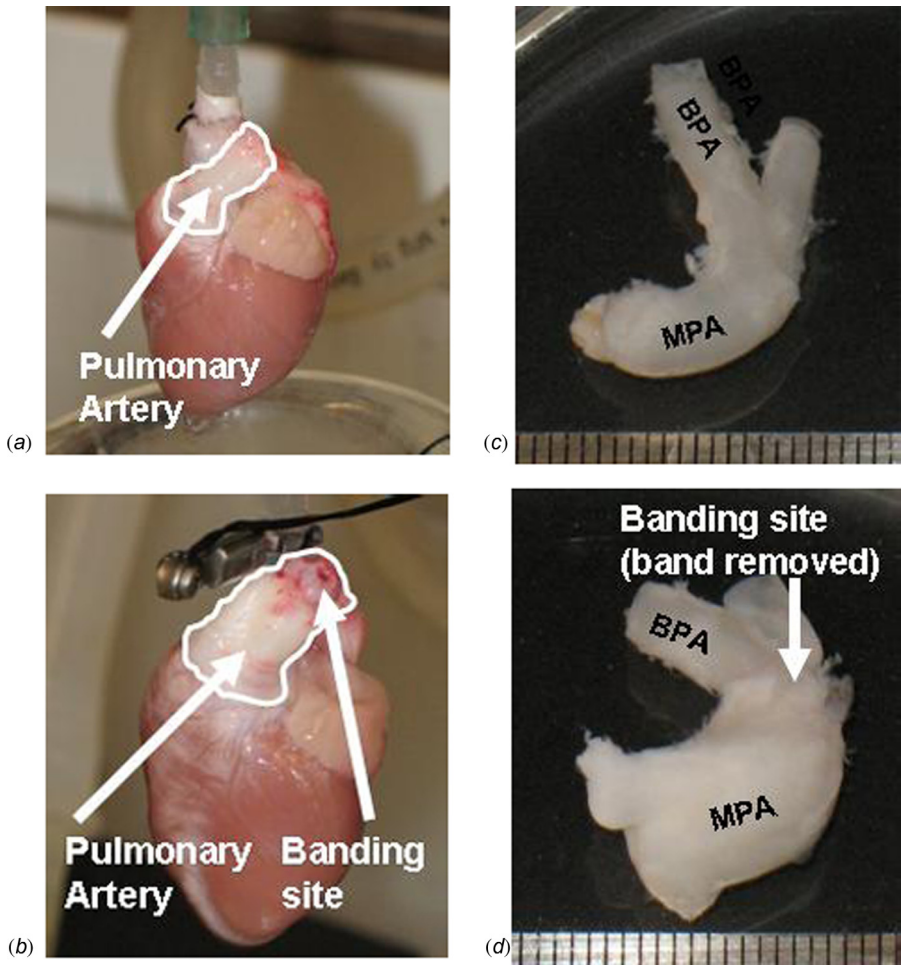

Fig. 1 Pictures of sham (*a*) and banded (*b*) PAs (outlined) during perfusion of the heart. Cleaned PAs from a sham (*c*) and banded (*d*) rabbit showing an increase in thickness and size of banded PAs. Arrows point to the banding sites in the banded PAs ((*b*) and (*d*)).

vascular biology, structure, and biomechanics. To this end, we studied the mechanical and biochemical changes both proximal (main PAs) and distal (branch PAs) to the obstruction after PA banding. Biaxial tensile testing was used to characterize the mechanical behavior of arteries. Collagen and elastin assays were performed for the quantification of biochemical changes in the ECM. Histology studies using Movat's pentachrome stain were used to examine changes in artery structure, and a pulsed Doppler technique was used to measure flow waves. Here we seek to relate the change in the mechanical properties of arteries with possible changes in microstructure and ECM components.

Materials and Methods

Pulmonary Artery Banding. The protocols used in this study were approved by the Institutional Animal Care and Use Committee at Children's Hospital Boston, and followed current NIH and American Physiologic Society guidelines. Main PAs in New Zealand white rabbits were banded as previously described [20]. Briefly, eleven rabbits at the age of 10–14 days weighing 176 ± 41 g were anesthetized with intramuscular injections of ketamine (50 mg/kg) and xylazine (2 mg/kg). After bupivacaine (0.1 mL) was injected subcutaneously, a left thoracotomy was performed through the third intercostal space. After the pericardium was incised, the main PA was isolated and banded with a 2–0 non-absorbable suture to constrict it by ~20% of its diameter. The chest cavity was closed by suturing the adjacent ribs together with a 3–0 suture. Air in the left chest was removed using a syringe with a 20-gauge catheter to complete expansion of the lungs. The chest and skin incisions were then closed with a 4–0 suture. Eleven rabbits were used for sham-operated controls (sham) and underwent an identical procedure except for the banding. Buprenorphine (0.01 to 0.05 mg/kg) was administered for pain immediately post operation or as needed.

Estimation of Pulmonary Artery Pressure by Doppler Echocardiography. Transthoracic echocardiography was performed at 8 weeks after surgery. The rabbits were sedated with intramuscular injection of ketamine (50 mg/kg) and xylazine (2 mg/kg). Doppler examination was performed with a commercially available echocardiograph (Philips Sonos 7500) utilizing a combined 2.25 MHz cross-sectional imaging/Doppler transducer. In the present study, the right ventricular systolic pressure was considered to be equivalent to pulmonary artery systolic pressure proximal to the binding site, although there are limitations to assessing PA pressure based on tricuspid regurgitation velocities [21]. Right ventricular systolic pressure was estimated when the tricuspid regurgitation was present, and color flow mapping was performed in multiple views to detect the presence of the tricuspid regurgitation. In the banded animals ($n = 11$), all had moderate to severe tricuspid regurgitation. Of the sham animals ($n = 11$), four had mild tricuspid regurgitation, and none was detectable in the others. A flow signal with the maximum spectral representation of high velocities and the Doppler cursor crossing the right chambers

(specifically not encroaching on the region of aortic outflow or left atrium) was recorded. The detected flow signal was examined by continuous-wave Doppler imaging, and a view providing the most complete flow envelopes and the highest peak velocity was selected. The peak right systolic pressure gradient was calculated from the highest peak velocity using the modified Bernoulli equation [22]. Right ventricular systolic pressure was calculated as the sum of the peak right systolic pressure gradient and the estimated right atrial pressure, which was assumed to be 10 mm Hg based on values from healthy infant rabbits [23,24].

Vessel Collection. The animals (sham weighing 2.20 ± 0.17 kg, banded weighing 2.10 ± 0.16 kg) were deeply anesthetized at ~8 weeks after banding (~10 weeks of age) with an intravenous injection of ketamine (100 mg/kg) and xylazine (5 mg/kg) via the marginal ear vein. The hearts were isolated and perfused in the Langendorff mode (Figs. 1(*a*) and 1(*b*)) as described previously [20]. Subsequently, the pulmonary arteries were separated from the heart and lungs and kept on ice. Vessels were then rinsed with de-ionized water and loose connective/fatty tissue was removed (Figs. 1(*c*) and 1(*d*)). The arteries were cut so an ~10 mm square sample was obtained from both the main and extralobar branch PAs. Samples were obtained from sham animals at similar regions. The squares were cut so one edge was parallel to the longitude of the artery while the other edge was parallel to the circumference of the artery. The thickness of each sample was measured at several locations with a pocket dial thickness gauge, and then the measurements were averaged. All main PAs from the 11 banded and 11 sham rabbits were successfully tested. Only seven branch PAs from banded rabbits and six branch PAs from the sham rabbits were tested successfully. The rest of the branch PAs failed mechanical testing due to their smaller size (~7 mm per side) and thickness (~0.2 mm). All the testing was performed within 24 h of harvesting.

Mechanical Testing. The biaxial tensile testing device had been previously used in many studies of soft tissue mechanics [25–28]. The edges of the tissue samples were connected to sandpaper tabs with cyanoacrylate glue (Elmer's Products, Ohio) and connected to the linear positioners with sutures. Samples remain in a bath of 1 x phosphate buffered saline solution (Fisher Scientific, Massachusetts) during mechanical testing. A load control protocol was implemented with a LabVIEW program, and load cells aligned with the two axes of movement. A small preload (2 ± 0.050 g) was applied in order to straighten the sutures connecting the tissue to the device. Initially each sample was put through a series of preconditioning cycles in which the sample was loaded in both directions to a 10 g load for branch PAs and 15 g load for main PAs. Eight cycles of equi-biaxial loads of 20–35 g to branch PAs and 45–75 g to main PAs were applied to study the anisotropic mechanical behavior of PAs. Maximum loads were chosen in order to recruit collagen fibers in the tissue and to fully capture the hyperelastic behavior of the arteries. However, the maximum loads were kept low enough so that tissue was not permanently damaged over the eight cycles. Data used for the analysis was collected from the eighth trial when the stress-strain curves had become stable. The displacement of four marker dots on the tissue was tracked with a CCD camera at 7–8 Hz to measure the strain as a result of the applied loads.

Stress-Strain Calculations. To calculate the stresses in the tissue, several assumptions were made. Because the thickness of the samples was much smaller than the length and width, a plane stress situation was assumed. In addition, the arteries were assumed to be incompressible [29] so the volume of the sample was considered to be conserved during the loading and unloading process. With these two assumptions, the Cauchy stress (load/deformed area) was

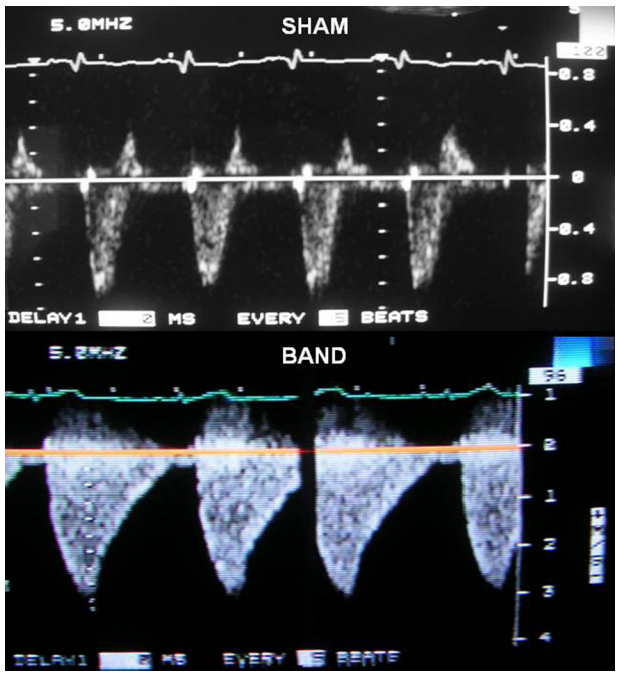

Fig. 2 Tricuspid regurgitation jet images showing longer decay time for banded (bottom) compared to sham (top) animals

determined using initial tissue dimensions and the load and stretch data from the biaxial testing device.

$$\sigma_1 = \frac{F_1 \lambda_1}{L_{2o} t}, \quad \sigma_2 = \frac{F_2 \lambda_2}{L_{1o} t} \tag{1}$$

In Equation 1, σ is the Cauchy stress, F is the applied load, λ is the stretch, L_o is the initial length, and t is the original thickness of the tissue. The subscripts *1*s and *2*s indicate the longitudinal and circumferential directions of the tissue, respectively. Logarithm strain (the natural logarithm of stretch) was used along with the Cauchy stress to describe the mechanical behavior of PAs [30].

In order to compare the stress strain curves, a linear region at the beginning section of the stress-strain curve was assumed, and the slope of this region (Fig. 6(*a*)) was defined as the "initial slope." The maximum slope of the stress-strain curve was

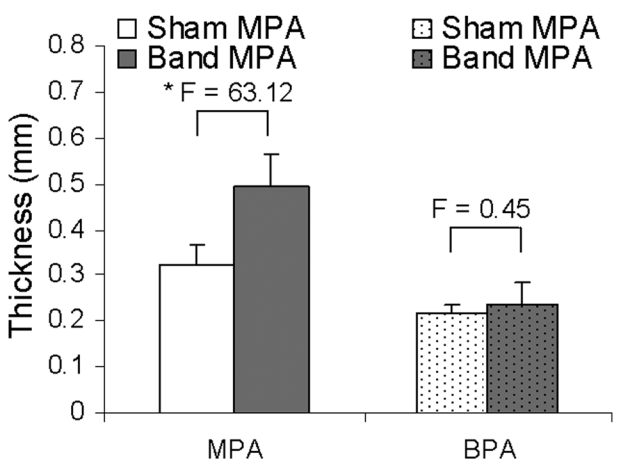

Fig. 3 Average thickness of sham and banded PAs. *p < 0.05.

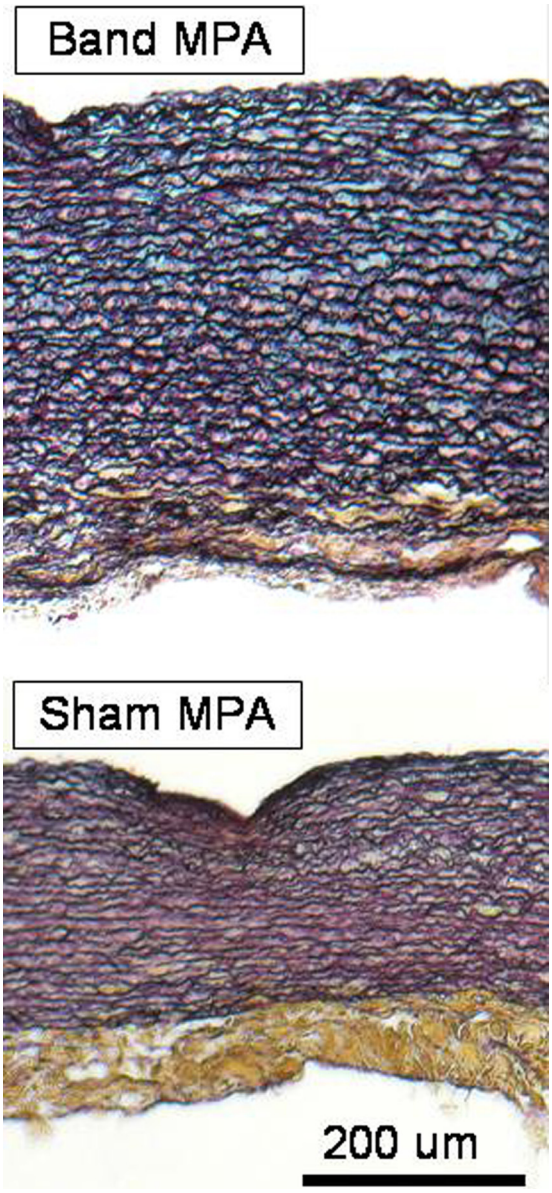

Fig. 4 Histological images of sham and banded main PAs using Movat's Pentachrome stain (cut along circumference of artery). Collagen fibers (yellow), smooth muscle cells/fibrin (red), ground substance (blue), and nuclei/elastic fibers (black). Scale bar is 200 um.

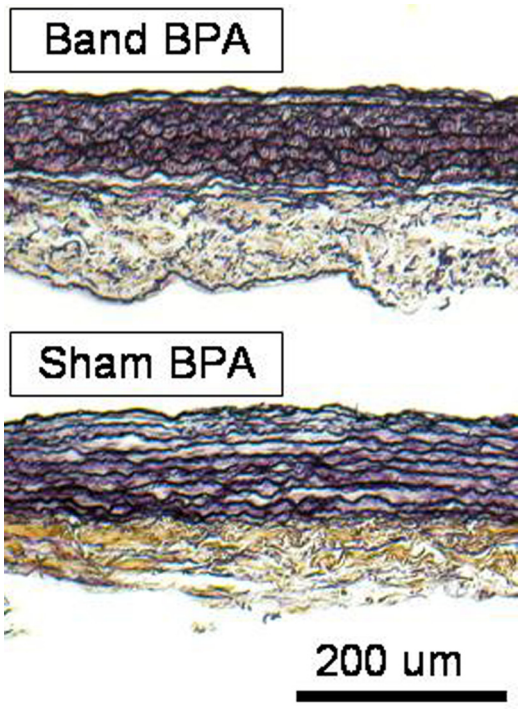

Fig. 5 Histological images of sham and banded branch PAs using Movat's Pentachrome stain (cut along circumference of artery). Collagen fibers (yellow), smooth muscle cells (red), ground substance (blue), and nuclei/elastic fibers (black). Scale bar is 200 um.

generally reached when the tissue was experiencing peak loads, and this was defined as the "stiff slope" (Fig. 6(*a*)) and was used for comparisons between banded and sham groups. The linearization of the initial and stiff regions was similar to what was done in previous literature [14,31–33]. In this study, the initial slope was consistently taken to include data points of slightly less than half of the total strain of the stress strain curve. For the stiff slope, we linearized a set of data recorded at the end of the loading cycle to approximate the stiff region of the curve without including the transition region. Also in Fig. 6(*a*) are the "knee points" of the circumferential and longitudinal directions. The knee point strain was determined by fitting the stress-strain curve with a 6^{th} order polynomial. After finding the local maximum in the curvature, the strain corresponding to the local maximum in curvature was defined as the "knee strain". The "knee stress" was found from the polynomial fit of the stress-strain curve [34].

Collagen and Elastin Assays. After mechanical testing, tissues were divided into smaller pieces for collagen and elastin assays. The amounts of salt soluble, pepsin soluble, and insoluble collagen were determined following the extraction procedures described in detail by Reddy [35]. After separating the volumes of different types of collagen, the samples were analyzed using a Sircol collagen assay kit following manufacture instructions (Biocolor). The Sircol collagen kit uses a quantitative dye-binding method that allowed for the determination of amounts of soluble and insoluble collagen. Absorbance was measured using a SpectraMax M5 plate reader (Molecular Devices) at a 540 nm wavelength and collagen content was expressed as ug of collagen/mg of wet tissue weight.

Elastin content in main and branch PAs was measured using Fastin elastin assay kit (Biocolor Ltd., Northern Ireland). Following manufacture's protocols, our assays measured soluble tropoelastins and insoluble elastin that was solubilized into α-elastin polypeptides. The optical density was measured at 513 nm using the microplate reader. Elastin content was expressed as ug of elastin/mg of wet tissue weight.

Histology Studies. Movat's pentachrome stain was used to identify differences in collagen, elastin, and ground substance in tissue [36,37]. Tissue samples were fixed in 10% formalin buffer and then embedded in paraffin. The tissue sample was then cut into $\sim$6 um cross-sectional slices for optical microscopy to view changes in the structure of the arteries in sham and banded animals.

Statistical Analysis. Experimental data were analyzed using a two-way mixed model factorial analysis of variance (ANOVA), where treatment (band or sham) and location (main or branch) were the two factors, and initial slope, stiff slope, knee stress, knee strain, amounts of collagen, and amounts of elastin in the

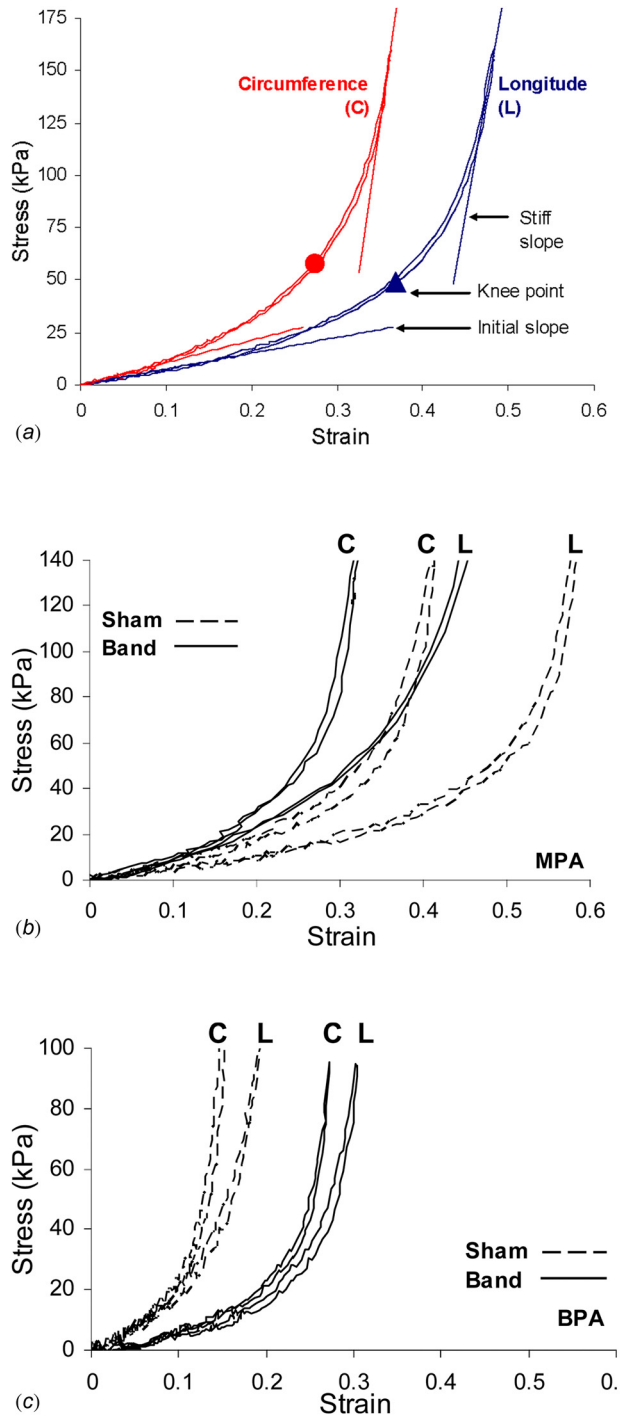

Fig. 6 (*a*) Example stress-strain curves showing the regions used to determine the initial and stiff slope along with the knee points. (*b*) Representative curves from the sham and banded main PAs. (*c*) Representative curves from the sham and banded branch PAs.

samples were the dependent variables [38]. A two-tailed value of $p < 0.05$ was considered statistically significant with post hoc testing done using the Fisher least significant difference (LSD) procedure. Results in the text were expressed as mean ± SD. In addition, Pearson correlation analyses were performed to determine the correlations between the stiff slopes in the main PAs with the total and cross-linked collagen. Statistical analysis was performed using the SPSS software package (version 18.0, SPSS Inc./IBM, Chicago, IL) and the JMP software (version 9.0.1, SAS Institute Inc., Cary, NC).

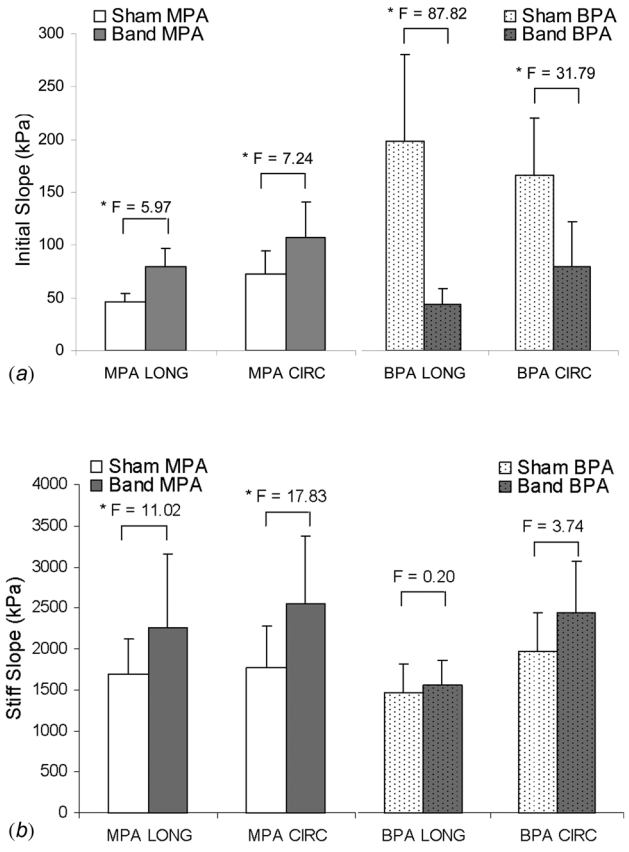

Fig. 7 Changes in initial slopes (*a*) and stiff slopes (*b*) in main and branch PAs. *p < 0.05.

Results

Wave Velocity and Estimated Pressure. Representative Doppler waves are presented in Fig. 2 with the velocity trace in m/s. The peak velocity in the sham animals is 0.75 ± 0.13 m/s while banded animals have a peak velocity of 2.67 ± 0.28 m/s. The waveform tracings suggest that the "flow packet" has a longer pressure decay time in banded animals than in sham animals. In addition, the majority of the blood flow occurs during the middle region of the systolic phase in banded animals. The sham animals have the majority of blood flow during the initial period of the systole, and then the flow decreases rapidly. As estimated from the peak velocity, eight weeks after surgery the pressure in the main PAs of the sham rabbits is 12.3 ± 2.2 mm Hg and 48.7 ± 3.3 mm Hg in the banded rabbits.

Structural Changes. The main PAs experience higher pressures due to the banding and become thicker after remodeling. As shown in Fig. 3, the banded main PAs have a significant increase in thickness compared to sham main PAs. The thicknesses of the branch PAs are not significantly different as a result of banding. Our histology studies show a loss of integrity of the media, increase in ground substance, and dispersion of collagen (Figs. 4 and 5). It was noted that the presence of collagen, especially in the medial layer, can be obscured by the presence of elastin/cells that are stained with a much darker color. The sham animals have a very distinct media layer composed of concentric rings of smooth muscle cells (red) and elastic lamina (black). The adventitia layer forms a clear outer wall of the artery and is composed of mostly irregularly arranged collagen bundles (yellow) in the sham animals. In the banded animals, there is deposition of elastic fibers between the concentric layers of elastic lamina as well as loss of a clear division between the media and adventitia.

In addition, in the media of both the main and branch sections of sham PAs, the concentric layers of smooth muscle cells are generally evenly spaced and the boundaries for each concentric layer are clearly separated by the elastic lamellae layers. On the contrary, the banded PAs appear to have more elastic fiber deposition within the layers of smooth muscle cells that cause the concentric layers to appear interconnected. There is also more ground substance (blue) mixed in with the smooth muscle cell layers in the media of the band main PAs.

Mechanical Changes. Figure 6(*a*) shows a representative set of stress-strain curves with the definition of slopes and knee points in the circumferential (C) and longitudinal (L) directions. Figures 6(*b*) and 6(*c*) show example plots from the main and branch regions, respectively. In both the main and branch PAs, there is anisotropic behavior with the circumferential directions being stiffer than the longitudinal directions.

In Fig. 7(*a*) are the initial slopes from the sham and banded arteries. Compared to the sham animals, the banded main PAs show a significant increase of slope in both the longitudinal and circumferential directions; however, the banded branch PAs show a significant decrease of slope in both directions. In Fig. 7(*b*) are the stiff slopes from the sham and banded PAs. For the banded main PAs, there is a significant increase in the longitudinal and circumferential direction stiff slopes. The banded PAs appear to

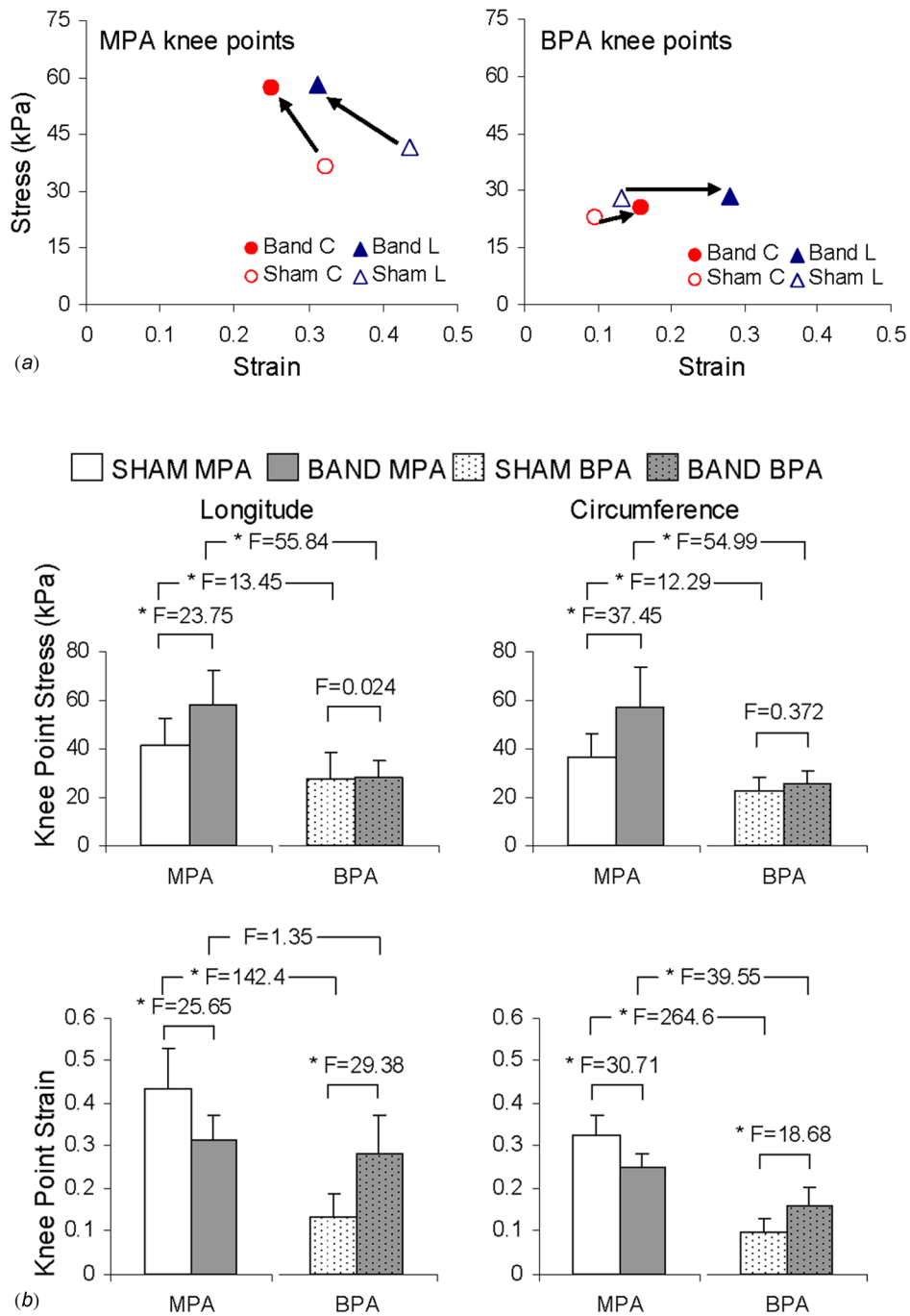

Fig. 8 (*a*) Knee points for sham and banded main and branch PAs showing the general shift that occurred. (*b*) Quantitative comparisons of the knee point stresses and strains along with F values corresponding to the comparisons indicated by the brackets. *p < 0.05.

Table 1 Summary of Mechanical Properties of Sham and Banded PAs

		Sham	Band	P	F
			Longitude		
MPA	Initial slope (kPa)	46.0 ± 8.8	79.6 ± 16.9	0.018	5.97
	Stiff slope (kPa)	1690.6 ± 429.8	2267.1 ± 899.1	0.001	11.02
	Knee strain	0.43 ± 0.92	0.31 ± 0.06	< 0.001	25.65
	Knee stress (kPa)	41.5 ± 10.9	58.0 ± 14.7	< 0.001	23.75
BPA	Initial slope (kPa)	200.0 ± 82.3	44.3 ± 15.0	< 0.001	87.82
	Stiff slope (kPa)	1464.2 ± 364.6	1567.5 ± 299.6	0.659	0.20
	Knee strain	0.13 ± 0.06	0.28 ± 0.09	< 0.001	29.39
	Knee stress (kPa)	27.8 ± 11.1	28.5 ± 6.9	0.876	0.024
			Circumference		
MPA	Initial slope (kPa)	73.5 ± 21.3	107.2 ± 33.6	0.009	7.24
	Stiff slope (kPa)	1764.5 ± 515.5	2549.0 ± 830.6	< 0.001	17.83
	Knee strain	0.32 ± 0.05	0.25 ± 0.04	< 0.001	30.71
	Knee stress (kPa)	36.5 ± 9.8	57.2 ± 16.9	< 0.001	37.45
BPA	Initial slope (kPa)	167.1 ± 54.9	80.5 ± 42.2	< 0.001	31.79
	Stiff slope (kPa)	1983.1 ± 476.5	2448.3 ± 635.4	0.57	3.74
	Knee strain	0.10 ± 0.03	0.16 ± 0.05	< 0.001	18.68
	Knee stress (kPa)	22.7 ± 5.4	25.6 ± 5.3	0.544	0.372

have increased stiff slopes in the longitudinal and circumferential directions when compared to the sham branch PAs, but the differences in the stiff slope of the branch PAs are not significant.

The banded main PA knee points on the left panel of Fig. 8(*a*) show a shift to a lower strain and higher stress in both longitudinal and circumferential directions compared to the sham main PA knee points. The right panel of Fig. 8(*a*) shows the shift in the branch PA knee points, and in banded groups there is an increase in strain with no change in stress. Quantitative comparisons of the shifts in the knee point stresses and strains are shown in Fig. 8(*b*). In the longitudinal and circumferential directions, the knee stresses increase significantly in the main PAs. The changes in the branch PA knee stresses are not significant. Also in Fig. 8(*b*), the longitudinal and circumferential knee strains decrease in the main PAs and increase in the branch PAs. A summary of the mechanical properties of the banded and sham PAs is presented in Table 1.

Biochemical Changes. In Fig. 9 are the results from the collagen assay where the soluble, insoluble, and total collagen are displayed. The soluble collagen is the sum of the salt and pepsin soluble collagen measurements. The total collagen is calculated by adding the soluble collagen with the insoluble collagen. In the main PAs, there is a significant increase in the amount of insoluble collagen in the banded groups ($P = 0.014$). In the branch PAs, there is a significant increase in the amount of pepsin soluble collagen in the banded groups ($P = < 0.001$). With banding, there is a significant increase in the total collagen in both the branch and main PAs ($P < 0.001$ and $P = 0.025$, respectively). A difference between the main and branch PAs is that in the main PAs, the greater amount of total collagen is caused by increased levels of insoluble collagen. In the branch artery tissue, the increase in total collagen is due to higher levels of soluble collagen ($P < 0.001$). The percent of cross-linked collagen is determined by dividing the amount of insoluble collagen by the total amount of collagen [35]. There is a significant increase in the percent of cross-linked collagen in the banded main PAs (from 33.9 ± 2.7% to 45.1 ± 6.8%, $P = 0.012$). The trend of decreasing percent of collagen cross-linking in the banded branch PAs is not significant (from 45.6 ± 6.3% to 41.2 ± 7.1%, $P = 0.398$).

There are no significant changes in the contents of total elastin between sham and banded groups in either the main (124 ± 37.6 μg/mg versus 148.2 ± 42.2 μg/mg, $P = 0.432$) or branch (146.2 ± 93.2 μg/mg versus 138.5 ± 67.2 μg/mg, $P = 0.796$) PAs. All values are reported as ug of elastin per mg of wet tissue weight.

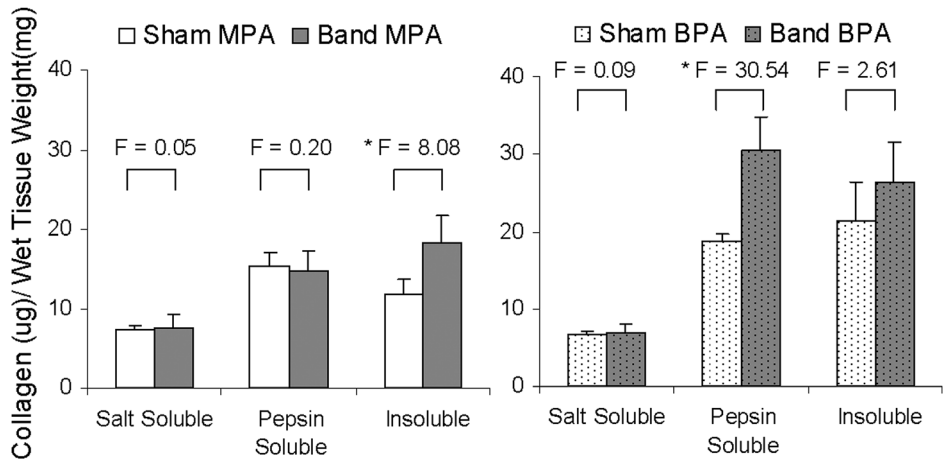

Fig. 9 Results of collagen assay showing the amounts of salt soluble, pepsin soluble, and insoluble collagen in the main (left) and branch (right) PAs. All values are reported as ug of collagen per mg of wet tissue weight. *p < 0.05.

Discussion

The main PAs experience higher pressures due to banding and become thicker after remodeling. This change in vessel size occurs similarly in the pulmonary arteries of hypertensive mice [13] as well as in the carotid arteries in human subjects with systemic hypertension [39]. Loss of integrity of the media is reported by previous studies on pulmonary and essential hypertension [37,40]. Increase in ground substance and the dispersion of the collagen in the main PA is found as a result of atherosclerosis and hypertension [41,42]. In addition to these structural alterations, elastin and collagen content will be discussed in relation to the changes in mechanical properties.

In the complex structure of an artery, the majority of the passive mechanical behavior is due to the collagen and elastin network while the SMCs provide the active contraction to facilitate blood flow [43,44]. In the initial region of loading, the elastin fibers bear the majority of the load and later the collagen fibers support the load in the stiff region [45,46]. The initial and stiff slopes are obtained with a goal of assessing the stiffness when elastin is the major load-bearing element, and after the strain stiffening when collagen fibers are recruited, respectively. Such information will allow us to begin to establish correlations between the structural and biomechanical changes in the PAs. With the current loading range and the thinness of the rabbit samples, the stress-strain curve reaches the stiffened region for each sample. The stiff slope is obtained in the stiffened region where the stress-strain relationship is relatively linear to minimize the effect of peak stress/strain on slope. However, due to sample-to-sample variations, the strain stiffening can happen over a wide range of strains [46]. It is also noted that the samples may reach different peak stresses/strains due to varying sample thickness, which may lead to comparing stress-strain slopes that occur over different strain ranges.

Our results show changes in the initial slopes of banded animals (Fig. 7(*a*)) without noticeable differences in elastin concentration. Other studies have also found that there is not a significant change in elastin content as a result hypertensive conditions on arteries [13,15,42]. While the total elastin content is unchanged, a possible cause for the differences of initial slope could be other modifications of the elastin network such as amount of cross-linking. Cross-linked elastin can be determined by measuring the amount of amino acids desmosines (DES) and isodesmosines (isoDES). Previous studies report an increase in cross-linking in the elastin network is correlated with an increase in the stiffness of tissue [47,48].

The stiff slope is defined in the region of the stress-strain curve where the collagen fibers have been mostly straightened and are supporting the load [46]. In the banded main PAs, there is an increase in stiff slope (Fig. 7(*b*)), total collagen, and cross-linked collagen compared to sham main PAs. With an increase in total collagen, various soft tissues display an increase in stiffness [32,49,50]. It also has been reported that when the collagen network is more cross-linked there is an increase in stiffness of the tissue [33,47,48], which coincides with our results for the main PAs. In the banded branch PAs, there is a significant increase in soluble and total collagen (Fig. 9). However, the change of the stiff slope (Fig. 7(*b*)) and percent of cross-linked collagen (Fig. 9) is not significant. The amount of insoluble and soluble collagen has been shown to affect the stiffness of the tendon in an opposite way [51]. We further plotted the correlations between the stiff slopes of MPA and the total and cross-linked collagen. Figure 10(*a*) shows that there is not a significant correlation between total collagen and stiff slope in either the circumferential ($P = 0.21$) or the longitudinal direction ($P = 0.16$). The correlation between collagen cross-linking and the stiff slope is significant in the circumferential direction ($P = 0.003$), but not in the longitudinal direction ($P = 0.15$) (Fig. 10(*b*)). This correlation between the circumferential stiff slope and collagen cross-linking has not been shown before. Although the total collagen content increases in both main and branch banded PAs, our results suggest that the percent of cross-linked collagen is a more reliable factor in determining the behavior of the stiff slope.

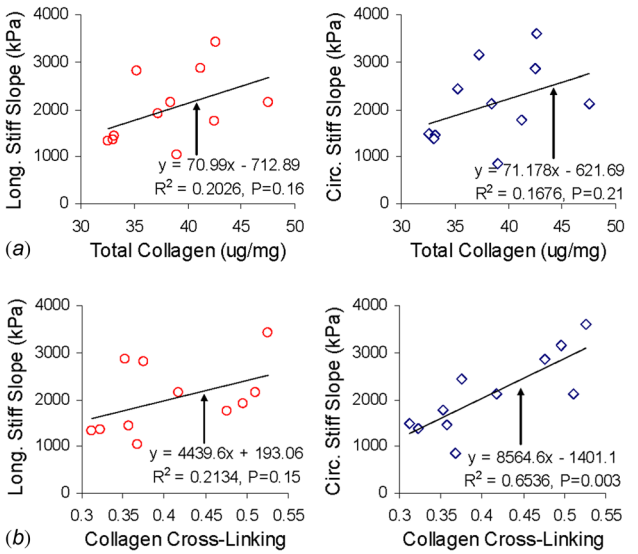

Fig. 10 Correlation plots (*a*) between stiff slope and total collagen and (*b*) between stiff slope and cross-linked collagen of main PA. Total collagen is reported as ug of collagen per mg of wet tissue weight.

The knee point gives an indication of when collagen starts becoming the primary load bearing ECM component in the PA. Shifting of the knee points to lower strains and higher stresses in the main PAs (Fig. 8) is similar to the changes in behavior of the arteries in spontaneously hypertensive rats (SHR) or hypoxia-induced hypertensive mice [13,15,52]. In those studies, there are increases in collagen levels without significant changes in the elastin content of the arteries, which leads to collagen recruitment at lower strain and an increase in stiffness [53]. This is confirmed by our biochemical assay results (Figs. 9), and so the main PAs appear to be undergoing similar structural remodeling as occurs in previous animal models of hypertension.

In contrast, the knee points of branch PAs shift to higher knee strain with no significant change in knee stress as a result of banding (Fig. 8). The shift of the branch knee points in this study is consistent with the decrease of initial slopes in the branch PAs. We expect that the changes in knee points should be due to combined effects of elastin and collagen ECM components in the artery. Unfortunately our current biochemical assay results are not sufficient to explain the right-ward shift of knee point strain for branch PAs. Although we did not find significant changes in elastin content, further biochemical studies on elastin cross-linking would be useful. Increased collagen deposition in arteries often coincides with calcium deposition in the ground substance, which can also affect the mechanical properties [40]. Obtaining such information should help better understand the structure-function remodeling in arteries.

While this study is focused on comparing the effects of the pulmonary obstruction between banded and sham groups, differences between the main and branch PAs are also evident from the data. In the sham animals, the branch PAs have significantly lower knee point stresses/strains compared to the main PAs as seen in Fig. 8(*b*). Similarly, other studies have reported decreases in elasticity in human arteries as the location of testing becomes more distal to the heart [54]. Increases in collagen content, decreases in elastin content, and increases in the collagen/elastin ratio have also been previously reported as arteries become more distal to the heart [54,55]. Our collagen assays show that the sham branch PAs have significantly higher amounts of total collagen compared to sham main PAs. However, elastin content is not significantly

different between the sham branch and main PAs. Because of this, the collagen/elastin ratio in the branch PAs is higher than in the main PAs, which provides a logical explanation for the knee point shifts.

Conclusions

Our study intends to investigate the relationship between mechanical integrity, microstructure, and biochemical composition of the arterial wall. To the best of our knowledge, this is the first study that determines changes in the mechanical and biochemical properties of PAs as a result of obstruction induced pulmonary vascular remodeling. Histology studies reveal a loss of integrity of the media. As a result of arterial remodeling, the initial slopes increase in the main PAs but decrease in the branch PAs, which cannot be explained by the lack of changes in elastin content. The stiff slopes in the main PAs of the banded rabbits increase, and this is attributed to the increase in collagen cross-linking. Shifting of the knee points in the main PAs are attributed to changes in collagen. The biochemical and mechanical changes reported in this study are likely to provide a better understanding of arterial remodeling when a PA obstruction(s) exists and/or pressure-flow characteristics are similarly affected. Future studies quantifying elastin cross-linking and direct PA pressure measurements would be useful in further illuminating the structure-function changes in remodeled arteries. In addition, studies involving more time points and a debanding/recovery process would create a better model of the arterial changes that occur due to an obstruction and after a treatment in patients.

Acknowledgment

This study was funded, in part, by research grants from the National Institutes of Health (Grant No. HL098028) and the National Science Foundation (Grant Nos. CAREER 0954825 and CMMI 1100791) to Y. Zhang.

References

[1] Lam, Y. Y., Kaya, M. G., Goktekin, O., Gatzoulis, M. A., Li, W., and Henein, M. Y., 2007, "Restrictive Right Ventricular Physiology: Its Presence and Symptomatic Contribution in Patients With Pulmonary Valvular Stenosis," J. Am. Coll. Cardiol., **50**, pp. 1491–1497.

[2] Petit, C. J., Gillespie, M. J., Harris, M. A., Seymour, T. L., Liu, T. Y., Khan, A., Gaynor, J. W., and Rome, J. J., 2009, "Relief of Branch Pulmonary Artery Stenosis Reduces Pulmonary Valve Insufficiency in a Swine Model," J. Thorac. Cardiovasc. Surg., **138**, pp. 382–389.

[3] Aburawi, E. H., Berg, A., and Pesonen, E., 2009, "Effects of Balloon Valvuloplasty on Coronary Blood Flow in Neonates With Critical Pulmonary Valve Stenosis Assessed With Transthoracic Doppler Echocardiography," J. Am. Soc. Echocardiogr., **22**(2), pp. 165–169.

[4] Hoshina, M., Tomita, H., Kimura, K., Ono, Y., Yagihara, T., and Echigo, S., 2002, "Factors Determining Peripheral Pulmonary Artery Stenosis Remodeling in Children After Percutaneous Transluminal Balloon Angioplasty," Circ. J., **66**, pp. 345–348.

[5] Freedom, R. M., Benson, L. N., Smallhorn, J. F., Williams, W. G., Trusler, G. A., and Rowe, R. D., 1986, "Subaortic Stenosis, the Univentricular Heart, and Banding of the Pulmonary Artery: An Analysis of the Courses of 43 Patients With Univentricular Heart Palliated by Pulmonary Artery Banding," Circulation, **73**, pp. 758–764.

[6] Hess, S. L., Bricker, J. T., Garson, A., Jr., Ott, D. A., Reul, G. J., and Cooley, D. A., 1992, "Pulmonary Artery Banding and Subaortic Stenosis in Patients With Single Ventricle: Surgical Alternatives and Clinical Outcome," Tex. Heart Inst. J., **19**(1), pp. 15–20.

[7] Rosenthal, A., Freed, M. D., Fyler, D. C., and Litwin, S. B., 1974, "Observations on the Development of Subaortic Stenosis Following Pulmonary Artery Banding," Chest, **65**, pp. 420–423.

[8] Saida, Y., Tanaka, R., Fukushima, R., Hira, S., Hoshi, K., Soda, A., Iizuka, T., Ishikawa, T., Nishimura, T., and Yamane, Y., 2009, "Histological Study of Right Ventricle-Pulmonary Artery Valved Conduit Implantation (RPVC) in Dogs With Pulmonic Stenosis," J. Vet. Med. Sci., **71**(4), pp. 409–415.

[9] Saida, Y., Tanaka, R., Fukushima, R., Hoshi, K., Hira, S., Soda, A., Iizuka, T., Ishikawa, T., Nishimura, T., and Yamane, Y., 2009, "Cardiovascular Effects of Right Ventricle-Pulmonary Artery Valved Conduit Implantation in Experimental Pulmonic Stenosis," J. Vet. Med. Sci., **71**(4), pp. 477–483.

[10] Orito, K., Yamane, T., Kanai, T., Fujii, Y., Wakao, Y., and Matsuda, H., 2004, "Time Course Sequences of Angiotensin Converting Enzyme and Chymase-Like Activities During Development of Right Ventricular Hypertrophy Induced by Pulmonary Artery Constriction in Dogs," Life Sci., **75**, pp. 1135–1145.

[11] Lima, C. O., Sahn, D. J., Valdes-Cruz, L. M., Goldberg, S. J., Barron, J. V., Allen, H. D., and Grenadier, E., 1983, "Noninvasive Prediction of Transvalvular Pressure Gradient in Patients With Pulmonary Stenosis by Quantitative Two-dimensional Echocardiographic Doppler Studies," Circulation, **67**, pp. 866–871.

[12] Foreman, J. E. K., and Hutchison, K. J., 1970, "Arterial Wall Vibration Distal to Stenoses in Isolated Arteries of Dog and Man," Circ. Res., **26**, pp. 583–590.

[13] Kobs, R. W., Muvarak, N. E., Eickhoff, J. C., and Chesler, N. C., 2005, "Linked Mechanical and Biological Aspects of Remodeling in Mouse Pulmonary Arteries With Hypoxia-Induced Hypertension," Am. J. Physiol. Heart Circ. Physiol., **255**, pp. H1209–H1217.

[14] Bruel, A., and Oxlund, H., 1996, "Changes in Biomechanical Properties, Composition of Collagen and Elastin, and Advanced Glycation end Products of the Rat Aorta in Relation to Age," Atherosclerosis, **127**(2), pp. 155–165.

[15] Boumaza, S., Arribas, S. M., Osborne-Pellegrin, M., McGrath, J. C., Laurent, S., Lacolley, P., and Challande, P., 2001, "Fenestrations of the Carotid Internal Elastic Lamina and Structural Adaptation in Stroke-Prone Spontaneously Hypertensive Rats," Hypertension, **37**, pp. 1101–1107.

[16] Gaballa, M. A., Jacob, C. T., Raya, T. E., Liu, J., Simon, B., and Goldman, S., 1998, "Large Artery Remodeling During Aging: Biaxial Passive and Active Stiffness," Hypertension, **32**, pp. 437–443.

[17] Martinez-Lemus, L. A., Hill, M. A., and Meininger, G. A., 2008, "The Plastic Nature of the Vascular Wall: A Continuum of Remodeling Events Contributing to Control of Arteriolar Diameter and Structure," Physiology, **24**, pp. 45–57.

[18] Meng, H., Wang, Z., Hoi, Y., Gao, L., Metaxa, E., Swartz, D. D., and Kolega, J., 2007, "Complex Hemodynamics at the Apex of an Arterial Bifurcation Induces Vascular Remodeling Resembling Cerebral Aneurysm Initiation," Stroke, **38**, pp. 1924–1931.

[19] Pistea, A., Bakker, E. N., Spaan, J. A., and VanBavel, E., 2005, "Flow Inhibits Inward Remodeling in Cannulated Porcine Small Coronary Arteries," Am. J. Physiol. Heart Circ. Physiol., **289**, pp. H2632–H2640.

[20] Kitahori, K., He, H., Kawata, M., Cowan, D. B., Friehs, I., Del Nido, P. J., and McGowan, F. X., Jr., 2009, "Development of Left Ventricular Diastolic Dysfunction With Preservation of Ejection Fraction During Progression of Infant Right Ventricular Hypertrophy," Circ. Heart Fail., **2**(6), pp. 599–607.

[21] Litwin, S. E., 2010. "Noninvasive Assessment of Pulmonary Artery Pressures: Moving Beyond Tricuspid Regurgitation Velocities," Circ. Cardiovasc. Imaging, **3**, pp. 132–133.

[22] Hatle, L., and Angelsen, B., 1982, *Doppler Ultrasound in Cardiology: Physical Principles and Clinical Application*, Lea and Febiger, Philadelphia, pp. 117–119.

[23] Minegishi, S., Kitahori, K., Murakami, A., and Ono, M., 2011, "Mechanism of Pressure-Overload Right Ventricular Hypertrophy in Infant Rabbits," Int. Heart J., **52**(1), pp. 56–60.

[24] Yock, P. G., and Popp, R. L., 1984, "Noninvasive Estimation of Right Ventricular Systolic Pressure by Doppler Ultrasound in Patients With Tricuspid Regurgitation," Circulation, **70**(4), pp. 657–662.

[25] Grashow, J. S., Yoganathan, A. P., and Sacks, M. S., 2006, "Biaxial Stress-Stretch Behavior of the Mitral Valve Anterior Leaflet at Physiologic Strain Rates," Ann. Biomed. Eng., **34**(2), pp. 315–325.

[26] Giles, J. M., Black, A. E., and Bischoff, J. E., 2007, "Anomalous Rate Dependence of the Preconditioned Response of Soft Tissue During Load Controlled Deformation," J. Biomech., **40**(4), pp. 777–785.

[27] Stella, J. A., Liao, J., and Sacks, M. S., 2007, "Time-Dependent Biaxial Mechanical Behavior of the Aortic Heart Valve Leaflet," J. Biomech., **40**(14), pp. 3169–3177.

[28] Zou, Y., and Zhang, Y., 2009, "An Experimental and Theoretical Study on the Anisotropy of Elastin Network," Ann. Biomed. Eng., **37**(8), pp. 1572–1583.

[29] Humphrey, J. D., Eberth, J. F., Dye, W. W., and Gleason, R. L., 2009, "Fundamental Role of Axial Stress in Compensatory Adaptations by Arteries," J. Biomech., **42**(1), pp. 1–8.

[30] Zhang, Y., Dunn, M. L., Drexler, E. S., McCowan, C. N., Slifka, A. J., Ivy, D. D., and Shandas, R., 2005, "A Microstructural Hyperelastic Model of Pulmonary Arteries Under Normo- and Hypertensive Conditions," Ann. Biomed. Eng. **33**(8), pp. 1042–1052.

[31] Stemper, B. D., Yoganandan, N., Stineman, M. R., Gennarelli, T. A., Baisden, J. L., and Pintar, F. A., 2007, "Mechanics of Fresh, Refrigerated, and Frozen Arterial Tissue," J. Surg. Res., **139**(2), pp. 236-242.

[32] Roeder, B. A., Kokini, K., Sturgis, J. E., Robinson, J. P., and Voytik-Harbin, S. L., 2002, "Tensile Mechanical Properties of Three-Dimensional Type I Collagen Extracellular Matrices With Varied Microstructure," J. Biomech. Eng., **124**(2), pp. 214–222.

[33] Bruel, A., Ortoft, G., and Oxlund, H., 1998, "Inhibition of Cross-Links in Collagen is Associated With Reduced Stiffness of the Aorta in Young Rats," Atherosclerosis, **140**, pp. 135–145.

[34] Madhavan, K., Belchenko, D., Motta, A., and Tan, W., 2009, "Evaluation of Composition and Crosslinking Effects on Collagen-Based Composite Constructs," Acta Biomater., **6**(4), pp. 1413–1422.

[35] Reddy, K. G., 2004, "AGE-Related Cross-Linking of Collagen is Associated With Aortic Wall Matrix Stiffness in the Pathogenesis of Drug-Induced Diabetes in Rats," Microvasc. Res., **68**(2), pp. 132–142.

[36] Taylor, A. J., Gorman, P. D., Farb, A., Hoopes, T. G., and Virmani, R., 1999, "Long-Term Coronary Vascular Response to 32P Beta-Particle-Emitting Stents in a Canine Model," Circulation, **100**, pp. 2366–2372.

[37] Arbustini, E., Morbini, P., D'Armini, A. M., Repetto, A., Minzioni, G., Piovella, F., Vigano, M., and Tavazzi, L., 2002, "Plaque Composition in Plexogenic and Thromboembolic Pulmonary Hypertension: The Critical Role

of Thrombotic Material in Pultaceous Core Formation. Heart, **88**(2), pp. 177–182.
[38] Sokal, R. R., and Rohlf, F. J., 1995, *Biometry: The Principles and Practice of Statistics in Biological Research*, 3rd ed. W. H. Freeman, New York, pp. 321–391.
[39] Puato, M., Palatini, P., Zanardo, M., Dorigatti, F., Tirrito, C., Rattazzi, M., and Pauletto, P., 2008, "Increase in Carotid Intima-Media Thickness in Grade I Hypertensive Subjects: White-Coat Versus Sustained Hypertension," Hypertension, **51**, pp. 1300–1305.
[40] Laurent, S., Boutouyrie, P., and Lacolley, P., 2005, "Structural and Genetic Bases of Arterial Stiffness," Hypertension, **45**, pp. 1050–1055.
[41] McDonald, T. O., Gerrity, R. G., Jen, C., Chen, H. J., Wark, K., Wight, T. N., Chait, A., and O'Brien, K. D., 2007, "Diabetes and Arterial Extracellular Matrix Changes in a Porcine Model of Atherosclerosis," J. Histochem. Cytochem., **55**, pp. 1149–1157.
[42] Briones, A. M., Xavier, F. E., Arribas, S. M., Gonzalez, M. C., Rossoni, L. V., Alonso, M. J., and Salaices, M., 2006, "Alterations in Structure and Mechanics of Resistance Arteries From Ouabain-Induced Hypertensive Rats," Am. J. Physiol. Heart. Circ. Physiol., **291**, pp. H193–H201.
[43] Dobrin, P. B., 1978, "Mechanical Properties of Arteries," Physiol. Rev., **58**(2), pp. 397–460.
[44] Fonck, E., Prod'hom, G., Roy, S., Augsburger, L., Rufenacht, D. A., and Stergiopulos, N., 2007, "Effect of Elastin Degradation on Carotid Wall Mechanics as Assessed by a Constituent-Based Biomechanical Model," Am. J. Physiol. Heart Circ. Physiol., **292**, pp. H2754–H2763.
[45] Cox, R. H., 1978, "Passive Mechanics and Connective Tissue Composition of Canine Arteries," Am. J. Physiol. Heart. Circ. Physiol., **234**, pp. H533–H541.
[46] Lally, C., Reid, A. J., and Prendergast, P. J., 2004, "Elastic Behavior of Porcine Coronary Artery Tissue Under Unixial and Equibiaxial Tension," Ann. Biomed. Eng., **32**(10), pp. 1355–1364.
[47] Yonter, E. O., Scott-Burden, T., and West, J. L., 1999, "Mechanical Properties of Tissue Engineered Constructs With Increased Crosslinking of the Extracellular Matrix," Proceedings of the First Joint BMES/EMBS Conference, Oct. 13–16, **1**, p. 129.
[48] Elbjeirami, W. M., Yonter, E. O., Starcher, B. C., and West, J. L., 2003, "Enhancing Mechanical Properties of Tissue-Engineered Constructs via Lysyl Oxidase Crosslinking Activity," J. Biomed. Mater. Res. Part. A, **66**(3), pp. 513–521.
[49] Vogel, H. G., 1974, "Correlation Between Tensile Strength and Collagen Content in Rat Skin: Effect of Age and Cortisol Treatment," Connect. Tissue Res., **2**, pp. 177–182.
[50] Lytle, I. F., Dhawan, V., Calve, S., Arruda, E. M., and Brown, D. L., 2007, "Tissue Engineered Tendons, Tensile Strength and Collagen Content Improve With in vivo Conditioning," J. Surg. Res., **137**(2), pp. 251–252.
[51] Reddy, K. G., 2004, "Cross-Linking in Collagen by Nonenzymatic Glycation Increases the Matrix Stiffness in Rabbit Achilles Tendon," Experimental Diab. Res., **5**, pp. 143–153.
[52] Briones, A. M., Gonzalez, J. M., Somoza, B., Giraldo, J., Daly, C. J., Vila, E., Gonzalez, M. C., McGrath, J. C., and Arribas, S. M., 2003, "Role of Elastin in Spontaneously Hypertensive Rat Small Mesenteric Artery Remodeling," J. Physiol., **552**(1), pp. 185–195.
[53] Intengan, H. D., Thibault, G., Li, J. S., and Schiffrin, E. L., 1999, "Resistance Artery Mechanics, Structure, and Extracellular Components in Spontaneously Hypertensive Rats: Effects of Angiotensin Receptor Antagonism and Converting Enzyme Inhibition," Circulation, **100**, pp. 2267–2275.
[54] Kumar, K., 2001, "Microstructure of Human Arteries," J. Anat. Soc. India, **50**(2), pp. 127–130.
[55] Harkness, M. L. R., Harkness, R. D., and McDonald, D. A., 1957, "The Collagen and Elastin Content of the Arterial Wall in the Dog," Proc. R. Soc. London, Ser. B, **146**(925), pp. 541–551.